Available online at www.sciencedirect.com
ScienceDirect
Trans. Nonferrous Met. Soc. China 35(2025) 2988−2999
Transactions of Nonferrous Metals Society of China
www.tnmsc.cn

Refinement of core-shell hybrid structure reinforced CuZr-based bulk metallic glass matrix composites via dealloying in metallic melt

Wei GUO[1,2], Long-feng LI[1], Zhen ZHANG[1], Mi ZHAO[3,4],
Jin-cheng WANG[2], Yan-qiang QIAO[2], Shu-lin LÜ[1], Shu-sen WU[1]

1. State Key Lab of Materials Processing and Die & Mould Technology, School of Materials Science and Engineering, Huazhong University of Science and Technology, Wuhan 430074, China;
2. State Key Laboratory of Solidification Processing, Northwestern Polytechnical University, Xi'an 710072, China;
3. School of Aerospace Engineering, Huazhong University of Science and Technology, Wuhan 430074, China;
4. Shenzhen Huazhong University of Science and Technology Research Institute, Shenzhen 518057, China

Received 16 January 2024; accepted 5 September 2024

Abstract: Metallic glass matrix composites (BMGCs) with compositions of $[(Zr_{0.5}Cu_{0.5})_{0.925}Al_{0.07}Sn_{0.005}]_{100-x}Ta_x$ (atomic fraction, %, x=3, 5, 7) were successfully prepared via dealloying in metallic melt. The reinforcing phase in these alloys has core-shell hybrid structure with Ta-rich particles as core and B2-CuZr as shell. In this method, the dealloyed Ta from Zr−Ta pre-alloys maintained in solid state and aggregated to form the fine Ta-rich phase in the final products. This effectively decreases the size of Ta-rich phase compared with that prepared via conventional arc-melting, where the Ta-rich phase was formed through dissolving and precipitation. Among the three compositions, $[(Zr_{0.5}Cu_{0.5})_{0.925}Al_{0.07}Sn_{0.005}]_{95}Ta_5$ showed the highest plastic strain of 11.2%, much higher than that of the arc-melted counterparts (4.3%). Such improvement in mechanical properties was related with the refined core-shell hybrid reinforcing structure, which could hinder the rapid propagation of main shear band more efficiently and cause them to branch and proliferate at the interface.

Key words: metallic glass matrix composites; core-shell hybrid reinforcement structure; dealloying in metallic melt; strength and toughness; B2-CuZr

1 Introduction

Owing to the long-range disordered atomic structure, bulk metallic glasses (BMGs) generally exhibit excellent properties, such as high fracture strength, large elastic limit, and excellent corrosion resistance. These superior properties make BMGs one kind of the promising candidates in a wide range of applications, including biomedicine, aerospace and electronic products [1−5]. However, most BMGs suffer from localized deformation under external loading, leading to the rapid propagation of main shear bands and resulting in brittle fracture behavior. To address this challenge, researchers have introduced a secondary phase into the amorphous matrix through ex-situ external addition or in-situ precipitation to fabricate bulk metallic glass matrix composites (BMGCs). Tailoring the composite structure is one effective approach in improving the room-temperature plasticity of BMGs [6−11]. Generally, the in-situ secondary phase exhibits stronger bonding with the amorphous matrix and yields a better mechanical performance compared with the ex-situ counterparts. However, the strain softening phenomenon after yielding for most BMGCs limits their applications.

To address this issue, PAULY et al [12] and WU

Corresponding author: Mi ZHAO, Tel: +86-27-87540185, E-mail: zhaomi2018@hust.edu.cn
https://doi.org/10.1016/S1003-6326(25)66861-0

et al [13] proposed the transformation-induced plasticity (TRIP) effect in BMGCs, where an in-situ metastable B2-CuZr phase precipitates in CuZr-based BMGCs. The B2-CuZr phase could not only induce shear band proliferation to improve the plasticity, but also trigger the stress-induced martensitic transformations during deformation and subsequently lead to the work-hardening behavior [14−16]. Nevertheless, the B2-CuZr phase tends to aggregate due to the inhomogeneous elemental distribution and the different local cooling rates in the samples, resulting in non-uniform distributed large blocks. Such heterogeneous composite structure degrades the mechanical properties of these work-hardenable BMGCs [17−19].

The introduction of heterogeneous nucleation substrate should bring about smaller and more homogeneous distributed B2-CuZr phase [6−10,13, 20,21]. For example, SONG et al [6] investigated the influence of TaW refractory particles on the dispersion of B2-CuZr. It was observed that larger high-melting-point particles promoted the nucleation of B2-CuZr and intensified its eutectic decomposition reaction. To date, the process designed to induce the in-situ nucleation substrates for B2-CuZr is still challenging and requires further extensive researches.

The ductile Ta is also one of the common reinforcing phases in BMGCs [8,22−25]. For example, the Ta-rich phase has been successfully introduced in a Zr−Cu−Ni−Al amorphous matrix to improve mechanical properties by the concentration of shear stress at the interfaces during the plastic deformation of Ta-rich phase. The existence of ductile Ta-rich phase adjusts the shear stress distribution and triggers multiple shear band formation. LIAO et al [8] improved the mechanical properties of BMGCs by homogenizing the distribution of B2-CuZr phases, where the ex-situ Ta particles were directly added. However, in their case, the fraction of Ta particles was very limited and the improvement in the mechanical properties is noteless. LIU et al [26] incorporated a small amount of Ta into a B2-CuZr phase formable CuZr-based BMGCs. Owing to Ta addition, the B2-CuZr phase became more uniform that significantly improved the mechanical properties. They also developed a partial core-shell structure with Ta-rich phase as core and B2-CuZr as shell to reinforce the CuZr-based BMGCs [27]. This gives a good idea for the design of reinforcing phases in BMGCs. However, due to the limited Ta content, the volume fraction of Ta-rich particles as well as the core-shell interface area, is far from enough to modify the overall mechanical behavior [27]. Hence, a more distinct core-shell reinforcing structure should be optimized.

In 2011, WADA et al [28] introduced the concept of liquid metal dealloying (LMD) reactions based on the following principle: in a binary (A−B) alloy, B can dissolve in C-melt (negative value of mixing enthalpy between B and C), while A cannot dissolve (positive value of mixing enthalpy between A and C). If A−B pre-alloy is immersed in C-melt, B will selectively dissolve into C-melt, separated from A−B alloy, and the remaining A diffuses and connects with pores inside. Meanwhile, the C−B melt infiltrates into these pores, promoting the continuous dealloying reactions in the inner part of A−B alloy. As a result, porous A with C−B filled in forms.

Our previous study [10,20] applied such dealloying in metallic melt to prepare the in-situ Ti-reinforced Mg-based BMGCs. We have also successfully prepared in-situ $[(Zr_{0.5}Cu_{0.5})_{0.925}Al_{0.07}Sn_{0.005}]_{100-x}Ta_x$ (atomic fraction, x=3, 5, 7) BMGCs with a core-shell hybrid reinforcement structure (Ta-rich phase as the core and B2-CuZr as the shell) [29]. In the present study, we tried to introduce the dealloying in metallic melt in the preparation of refined core-shell hybrid reinforced BMGCs. Based on the relations in mixing enthalpy between elements, we designed to induce the dealloying by immersing Zr−Ta pre-alloy in a Cu−Al−Sn melt, where Zr from the pre-alloy can selectively into the Cu−Al−Sn melt and give rise to the B2-CuZr formable target Zr−Cu−Al−Sn melt. The remaining Ta in Zr−Ta should diffuse and collapsed to form Ta-rich reinforcing phase. Due to the low content of Ta in Zr−Ta pre-alloy, fine Ta-rich phase can be obtained after the collapse of ligament from the structure of high porosity. Following such theoretical design, we conducted a detailed investigation in the microstructure and mechanical properties of core-shell hybrid structure reinforced BMGCs with different Ta contents. The counterparts prepared by conventional arc-melting process, where Ta was firstly dissolved and then precipitated during solidification, were also fabricated for comparison.

2 Experimental

The compositions of the BMGCs were designed to be $[(Zr_{0.5}Cu_{0.5})_{0.925}Al_{0.07}Sn_{0.005}]_{100-x}Ta_x$ (atomic fraction, x=3, 5, 7). The raw materials of Cu, Zr, Al, Sn, and Ta pieces were used with purities exceeding 99.99 wt.%. Firstly, arc-melting was conducted in a water-cooled copper mold to fabricate Zr−Ta and Cu−Al−Sn pre-alloys under an argon atmosphere. Subsequently, Zr−Ta pre-alloy was mixed with Cu−Al−Sn pre-alloy by induction melting in a BN crucible under an argon atmosphere (melting/dealloying temperature ~1473 K for 2 min) to fabricate the master alloy ingots. During the induction heating, the dealloying reactions in metallic melt occurred. Then, the molten alloy was cast into a 30 mm-diameter copper mold to fabricate Zr−Cu−Al−Sn−Ta master alloy. On the other hand, the conventional arc-melting was employed to mix the two pre-alloys to fabricate the master alloys. During each arc-melting process, the alloy was held at a molten state for 3 to 5 min. To ensure the chemical homogeneity, the alloy was flipped and melted at least four times. Finally, the obtained master alloys were subjected to injection copper mold casting to fabricate cylindrical BMGC specimens with a diameter of 2 mm and a length of 60 mm. The $[(Zr_{0.5}Cu_{0.5})_{0.925}Al_{0.07}Sn_{0.005}]_{97}Ta_3$, $[(Zr_{0.5}Cu_{0.5})_{0.925}Al_{0.07}Sn_{0.005}]_{95}Ta_5$ and $[(Zr_{0.5}Cu_{0.5})_{0.925}Al_{0.07}Sn_{0.005}]_{93}Ta_7$ samples prepared using the dealloying method were labeled as Ta3-De, Ta5-De and Ta7-De, respectively, while those prepared through conventional arc-melting process as Ta3-Arc, Ta5-Arc and Ta7-Arc, respectively.

The structures of the samples were examined by X-ray diffraction (XRD 6100) with Cu K_α radiation. The microscopic morphology and fracture surfaces of the samples were observed by scanning electron microscope (GeminiSEM300) equipped with an energy dispersive X-ray spectrometer (EDS, X-Max 50) with an energy resolution better than 127 eV. The sample for SEM was cut from the lower end of the cylindrical specimens, inlaid in epoxy resin, and then polished for observation. Compression tests were conducted at room temperature with universal material testing machine (Zwick Z020) at a strain rate of 5×10^{-4} s^{-1}. The compression specimens were cylindrical with a diameter of 2 mm and a length of 4 mm, featuring with smooth and flat ends. To ensure the reproducibility, at least 6 specimens were tested for each sample.

3 Results and discussion

3.1 Microstructures of BMGC samples

Figure 1 shows the XRD patterns of Ta3-Arc, Ta3-De, Ta5-Arc, Ta5-De, Ta7-Arc and Ta7-De samples. All samples exhibit a prominent board

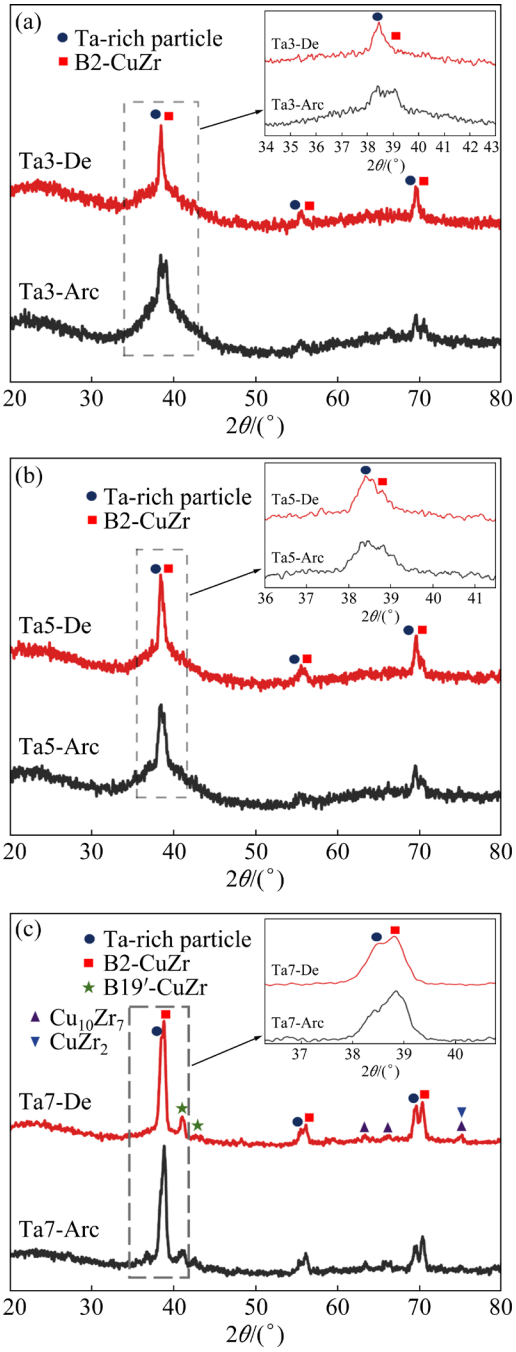

Fig. 1 XRD patterns of samples with different Ta contents under two processes

peak in the range between 30° and 45°, corresponding to their amorphous matrix. Diffraction peaks representing the Ta-rich phase and B2-CuZr phase can be observed around 38°, 56° and 70°, respectively. Besides, peaks of some unexpected crystalline phases such as B19′-CuZr, $Cu_{10}Zr_7$ and $CuZr_2$ are also detected in Ta7-Arc and Ta7-De. This should be related with the degraded GFA of the matrix with high Ta content. With increasing Ta addition, large amount of Ta can be dissolved in the matrix to facilitate the precipitation of Ta-rich phase. In this case, more and more Al can be segregated into the Ta-rich phase due to the negative mixing enthalpy between Al and Ta. As a result, the concentration of Al decreases in the matrix. Such alteration of Ta and Al in the matrix reduced its GFA and promoted the precipitation of the crystalline phases. Whatever, the XRD results demonstrate that the phase constitution of samples with the same composition are very similar no matter they were prepared via arc melting or dealloying method.

Figures 2(a, c, e) show the BSE (backscattered electron) images of Ta3-Arc, Ta5-Arc and Ta7-Arc, respectively. A substantial amount of Ta-rich phase is distributed on the amorphous matrix with B2-CuZr phase precipitating around. The Ta-rich phase is equiaxed in Ta3-Arc and Ta5-Arc, but it changes to dendritic in Ta7-Arc. In addition, the fraction of B2-CuZr phase increases in the sample with high Ta content due to the degraded GFA. Such high fraction also causes the aggregation of B2-CuZr phase. Moreover, B19′-CuZr can be also detected in Ta7-Arc. Due to the lower thermal conductivity of Ta-rich phase compared with the matrix, a residual heat-affected zone forms around the interface between them and contributes to the generation of B19′-CuZr phase during the cooling process. Furthermore, the deep gray $Cu_{10}Zr_7$ phase is also observed in Ta7-Arc, which may relate with the degraded GFA as discussed above.

Figures 2(b, d, f) show the BSE images of Ta3-De, Ta5-De and Ta7-De, respectively. The most noticeable features are the significant refined and more uniformly distributed Ta-rich phase compared with their arc-melted counterparts. The dendritic Ta-rich phase is no longer exists even in the sample with high Ta content. This refined Ta-rich phase acts as effective heterogeneous nucleation sites for the B2-CuZr phase, giving rise to an increased number density of core-shell hybrid reinforcing structures. In the upper right corner of each image, a highly magnified view highlights the core-shell hybrid reinforcing structure formed through dealloying. This close-up view reveals the detailed structures of the core and the shell phases. The core phase is distributed in a spherical pattern, while the shell phase is evenly distributed around the spherical core. Such observation agrees well with our design, confirming the expected refinement effect of the dealloying method on the core-shell hybrid reinforcing structure. Figures 2(g, h) show the EDS results for Ta5-Arc and Ta5-De, respectively. It can be seen from the embedded composition table that Points *A*−*C* refer to the amorphous matrix, the B2-CuZr phase, and the Ta-rich phase, respectively. The unexpected crystalline phase is detected, as shown in Point *D* for Ta5-Arc.

To further analyze the variations of the refinement effects in the samples with different Ta contents, the average size of Ta-rich phase was statistically analyzed using Image-Pro Plus software. It is found that as the Ta content increased, the Ta-rich phase in samples prepared by arc melting exhibited significant coarsening. In Ta7-Arc, the average size of the Ta-rich phase was about 17.9 μm, two times that in Ta3-Arc (~9.1 μm). However, the Ta-rich phase did not apparently coarsen with increasing Ta content in samples prepared by dealloying. In Ta7-De, the average size of the Ta-rich phase was about 4.0 μm, which was only 25% larger than that in Ta3-De (~3.2 μm). This phenomenon is attributed to the low reaction temperature (significantly below the melting point of Ta) during the dealloying process. As a result, Ta did not melt and re-precipitate. Instead, Zr from the Zr−Ta pre-alloy was selectively dissolved into the melt (dealloying reaction), leaving Ta to aggregate together by diffusion. For the low atomic fraction of Ta in Zr−Ta pre-alloys, these Ta atoms could not form complete pore structures but collapsed into fine particles in the melt. Subsequent injection casting processes still maintain such low temperatures to ensure that the fine Ta-rich phase did not dissolve and re-precipitate. As a result, the fine Ta-rich phase can be found in the composites fabricated by dealloying reaction even at high Ta contents.

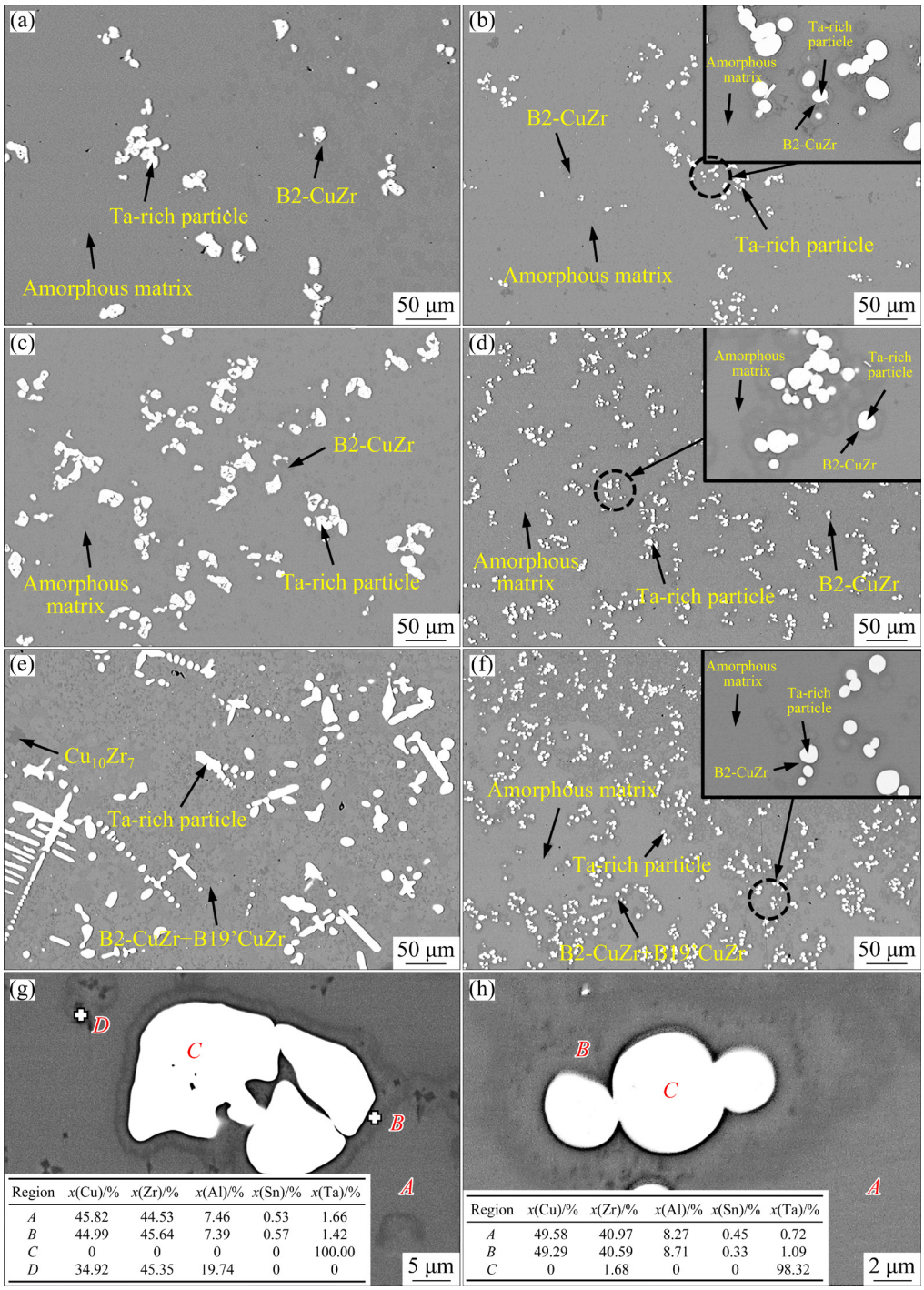

Region	x(Cu)/%	x(Zr)/%	x(Al)/%	x(Sn)/%	x(Ta)/%
A	45.82	44.53	7.46	0.53	1.66
B	44.99	45.64	7.39	0.57	1.42
C	0	0	0	0	100.00
D	34.92	45.35	19.74	0	0

Region	x(Cu)/%	x(Zr)/%	x(Al)/%	x(Sn)/%	x(Ta)/%
A	49.58	40.97	8.27	0.45	0.72
B	49.29	40.59	8.71	0.33	1.09
C	0	1.68	0	0	98.32

Fig. 2 BSE images of Ta3-Arc (a), Ta3-De (b), Ta5-Arc (c), Ta5-De (d), Ta7-Arc (e) and Ta7-De (f), and corresponding EDS results of Ta5-Arc (g) and Ta5-De (h)

The volume fractions of Ta-rich phase in Ta3-De, Ta5-De and Ta7-De are found to be 1.3%, 2.8% and 4.3%, respectively. It is noted that a higher Ta content results in a higher volume fraction of Ta-rich phase. We also further measured the size ratio of the core-shell in these samples. It is found that the core-shell size ratios (size of B2-CuZr phase to Ta-rich phase) were 1.9 for Ta3-De, 2.7 for Ta5-De, and 2.1 for Ta7-De. The finest particle of Ta-rich phase in Ta3-De may decrease the effective nucleation area for B2-CuZr phase, generating a finer B2-CuZr phase. Meanwhile, the more dissolved Ta in the matrix for Ta7-De degrades the B2-CuZr phase formality. Thus, the largest core-shell size ratio is obtained in Ta5-De. Moreover, we also calculate the volume

fraction of B2-CuZr phase based on the size ratio and the volume fraction of Ta-rich phase. It is also found that Ta5-De possessed the highest volume fraction of B2-CuZr phase (~22%), much higher than that of Ta3-De (~1.4%) and Ta7-De (~13.9%). However, despite of the refinement of the Ta-rich phase via dealloying reaction, the distribution of the B2-CuZr phase did not become more uniform in Ta7-De. Instead, large amount of B2/B19′ phases appeared in the center of the sample. Even though the influence of residual thermal stress at the interface was reduced due to the refinement of Ta-rich phase in Ta7-De, the higher Ta content causes more Ta to dissolve into the B2-CuZr phase and subsequently degrades its thermal stability. Thus, the B2-CuZr phase is more likely to transform to B19′-CuZr phase.

From above discussion, the optimal composite structure is obtained when Ta content is set to be 5 at.%. In Ta5-Arc and Ta5-De, unexpected phase is hardly formed and the faction of Ta-rich phase is relatively high. Thus, we further compared the microstructure between Ta5-Arc and Ta5-De to clarify the refinement effect of dealloying reactions. Figure 3 presents the statistical results and fitted curves for the size distribution of Ta-rich phase in Ta5-Arc and Ta5-De. The size distribution of Ta-rich phase in Ta5-Arc is much broad, ranging from a few micrometers to a maximum of 24 μm. In contrast, the size distribution of the Ta-rich phase in Ta5-De is narrower, indicating better uniformity in the sample. Meanwhile, the higher content of B2-CuZr phase and larger size ratio of core-shell structure in Ta5-De samples will contribute to more obvious work hardening and plastic deformation.

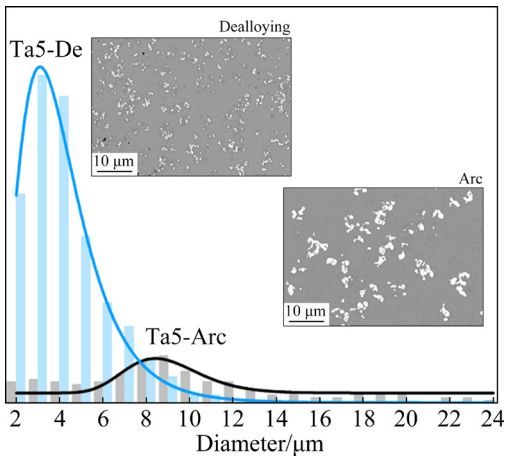

Fig. 3 Size distribution of Ta-rich phase in Ta5-Arc and Ta5-De

The statistical results further confirm the significant effect of the dealloying method in refining and making the core-shell hybrid reinforced structure uniformly distributed, which is expected to greatly improve the mechanical properties of the BMGCs.

3.2 Mechanical properties of BMGC samples

Figure 4(a) shows the compressive stress−strain curves of the BMGCs prepared using different methods, and the detailed mechanical data are summarized in Table 1. The improved mechanical properties from Ta3-Arc to Ta3-De, and

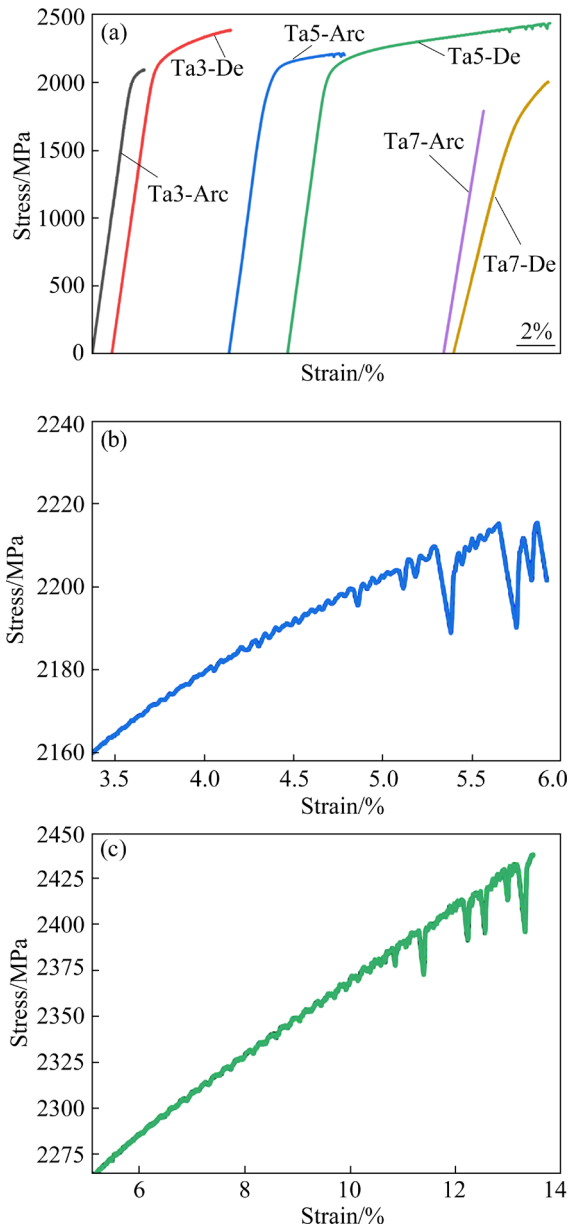

Fig. 4 Compressive stress−strain curves of Ta3-Arc, Ta3-De, Ta5-Arc, Ta5-De, Ta7-Arc and Ta7-De (a), and enlarged curves after yielding for Ta5-Arc (b) and Ta5-De (c)

Table 1 Mechanical properties (yield strength σ_y, fracture strength σ_f, fracture strain ε_f, and plastic strain ε_p) for samples

Sample	σ_y/MPa	σ_f/MPa	ε_f/%	ε_p/%
Ta3-Arc	1927±10	2090±10	2.2±0.1	0.7±0.1
Ta3-De	1904±10	2383±10	6.2±0.1	4.1±0.1
Ta5-Arc	1718±10	2214±10	5.9±0.1	4.3±0.1
Ta5-De	1898±10	2439±10	13.5±0.1	11.6±0.1
Ta7-Arc	1793±10	1793±10	2.1±0.1	−
Ta7-De	1487±10	2008±10	4.9±0.1	2.2±0.1

from Ta5-Arc to Ta5-De tell the advantages of dealloying process due to the refinement of core-shell hybrid structure. Ta3-De exhibits an ultimate strength of 2383 MPa and a plastic strain of 4.1%, higher than those of Ta3-Arc (2090 MPa and 0.7%). Ta5-De demonstrates an ultimate strength of 2439 MPa and a plastic strain of 11.6%, while those of Ta5-Arc are 2214 MPa and 4.3%. In contrast, due to the formation of unexpected hard phases and the transformed B19′-CuZr from B2-CuZr in Ta7-Arc and Ta7-De, the plastic strain is largely impaired.

Figures 4(b) and (c) are the enlarged stress−strain curves after yielding for Ta5-Arc and Ta5-De, respectively. Both figures show the obvious stress drops at the plastic deformation stage. It is noted that the stress drop is related with the initiation of shear bands, thus the serrated flow corresponds to the improved plasticity. Furthermore, the average value of such stress drop of Ta5-De is lower than that of Ta-Arc, indicating a lower energy barrier to initiate the shear bands and subsequent a more pronounced plastic deformability.

Figure 5(a) illustrates the overall side view of the fractured Ta5-De, which exhibits a fracture angle of 43° and demonstrates a typical shear fracture mode of amorphous matrix composite materials. Figure 5(b) shows the lateral surface of fractured Ta5-De with high magnification, revealing multiple shear band features. This phenomenon arises due to the obstruction of rapid propagation of the primary shear band within the amorphous matrix by the dual-phase core-shell reinforcement, causing it to halt, branch, and proliferate [12,30,31]. The initiated shear bands deflect or proliferate into numerous small secondary shear bands at the interface between the matrix and the secondary phase. The interaction between densely distributed shear bands effectively impedes the instability transition of the primary shear band towards crack initiation. Given that each shear band corresponds to a certain amount of plastic deformation, the formation of multiple shear bands enhances the room temperature plastic deformability of the BMGCs [32,33].

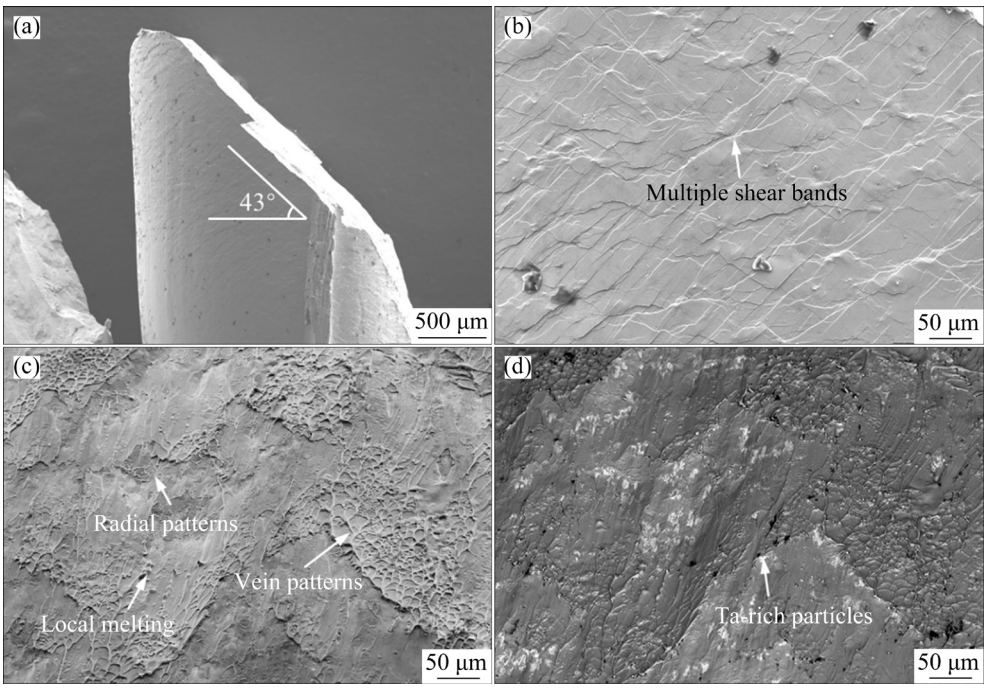

Fig. 5 SE images (a−c) and BSE image (d) of fracture surface of Ta5-De: (a, b) Lateral surface; (c, d) Fracture surface

Figures 5(c, d) present the secondary electron (SE) and the BSE images of the fracture surface, respectively. They display the characteristic radial patterns and vein patterns of amorphous alloys. Additionally, tear-drop-shaped locally melted regions and dispersed areas enriched in Ta phase are observed. The radial patterns often appear around the Ta-rich phase (see Fig. 5(d)), indicating that the core-shell hybrid structure with lower hardness (compared with the amorphous matrix) may undergo yielding and deform prior to the BMGCs [34]. This structure dissipates the high strain field and stress concentration formed at the interface, effectively retarding crack initiation. The semi-lunar vein pattern, accompanied by localized melting, exhibits a very fine size, signifying the inhibition of microcrack propagation. The formation of locally melted regions is attributed to the accumulation of shear bands in certain regions, where the destruction of rupture releases high elastic strain energy instantaneously. It leads to a rapid increase in the local temperature, causing softening and ultimately resulting in the formation of locally melted regions. Generally, such fracture regions are considered to be a characteristic feature of BMGCs with extensive plastic deformation [35].

To provide a more detailed explanation of the reinforcement mechanism of the present core-shell hybrid structure reinforced BMGCs, the compression test was performed using Ta5-De with side surface polished to mirror end. Figure 6(a) shows a low-magnification BSE image near the fracture surface, where multiple shear bands are observed to undergo various changes in direction and proliferation. A significant number of multiple shear bands exhibit an intertwined distribution, indicating that the core-shell hybrid structure effectively impedes the rapid propagation of shear bands and the generation of destructive cracking. High-magnification SEM observation of the fracture morphology reveals that the shear bands cannot directly penetrate the B2-CuZr phase and the Ta-rich phase. Multiple shear bands are observed at the interface between the amorphous phase and the B2-CuZr phase, as well as that between the Ta-rich phase and the B2-CuZr phase, as illustrated in Figs. 6(b, c). Additionally, noticeable deformation and even fracture are observed in the Ta-rich phase, suggesting that both the core phase (Ta-rich phase) and the shell phase (B2-CuZr phase) facilitate shear band halting, branching, and proliferation. Moreover, such deformation in Ta-rich phase also releases the stress concentration at the interface, thereby mitigating the strain softening of the amorphous matrix.

Based on the size and volume fraction of the core-shell reinforcing structure, the mean interphase spacing is determined by

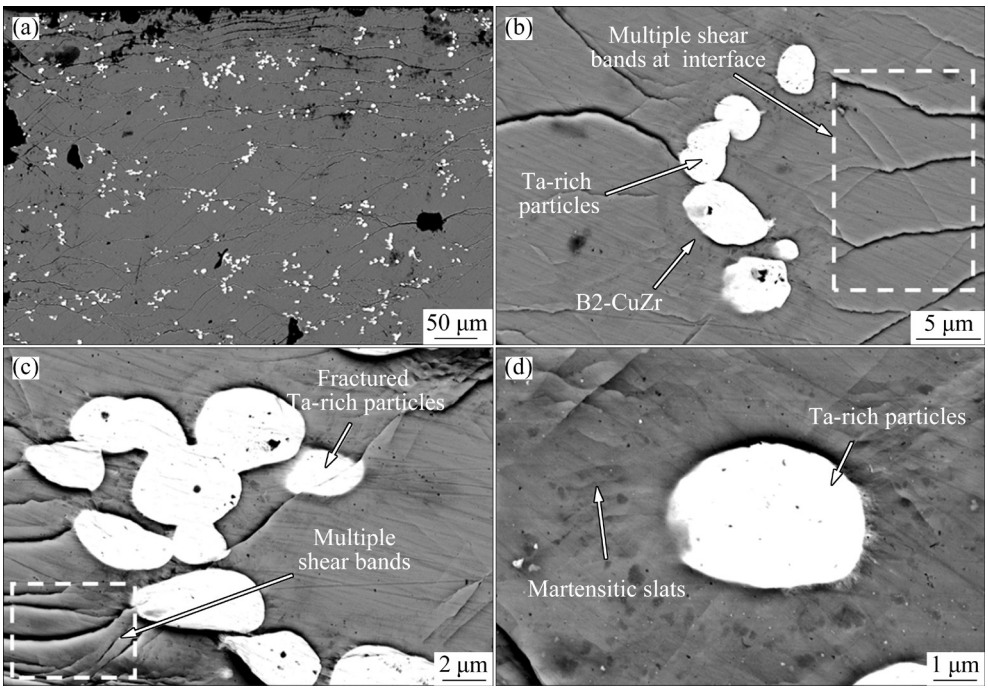

Fig. 6 BSE images of lateral surface of fractured polished Ta5-De with different magnifications

$$\lambda = d\sqrt[3]{\frac{\pi}{6f}} \quad (1)$$

where λ is the interphase spacing, d is the size of the core-shell structure, and f is the volume fraction of the core-shell structure. The calculated results indicate that Ta5-De has the smallest interphase spacing of ~2.6 μm. This should effectively lower the mean free path of shear bands. As a result, a more severer interaction between shear bands with the reinforcing phases generates, subsequently contributing to a more profound shear band multiplication.

Moreover, plate-like martensitic phases can be observed around the Ta-rich phase (Fig. 6(d)), indicating the stress-induced martensitic transformation during deformation. Figure 7 gives the XRD patterns of the samples before and after compression. It can be seen that diffraction peaks corresponding to the B19′-CuZr phase appear in the fractured sample, accompanied by a decrease in the peak intensity of the B2-CuZr phase. This indicates that the body-centered cubic B2-CuZr phase undergoes a martensitic transformation to form the harder B19′-CuZr phase under stress. The phase transformation induced hardening compensates for the softening of the amorphous matrix, thereby improving the overall mechanical properties of the BMGCs [36,37]. Simultaneously, the phase transformation of B2-CuZr during deformation releases the stress concentration in its vicinity and restricts the accumulation of free volume, further impeding the rapid expansion of shear bands. Finally, high stress is required to generate the

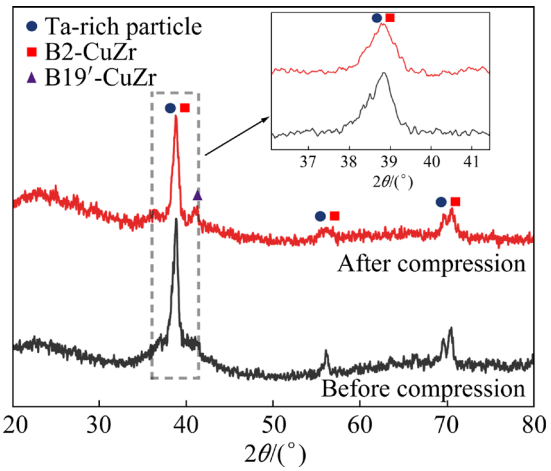

Fig. 7 XRD patterns of Ta5-De before and after compression

continuous expansion of shear bands, suppressing early necking and softening of the BMGCs [8,38].

Compared with a monolithic reinforcing phase, the core-shell hybrid structure exhibits a unique synergy strengthening effect. This is because that the differences in the elastic modulus and yield strength among the Ta-rich phase, B2-CuZr phase and amorphous matrix [16,34] result in non-uniform volumetric deformation under stress. The yield strength of the Ta-rich phase is relatively low [34]. Therefore, the deformation in Ta-rich phase should preferentially occur in the early stage of strain. This releases the stress concentration at the interface between the Ta-rich phase and the B2-CuZr phase, slowing down the initiation of early microcracks and allowing for the release of strain in the shell phase (B2-CuZr phase). As high stress is applied, the deformation of the B2-CuZr phase or even martensitic transformation leads to local volume changes and contributes to the further deformation in Ta-rich phase. It can absorb energy and facilitate work-hardening behavior.

The non-uniform volumetric deformation among different phases also induces internal stresses in the B2-CuZr phase, producing a more complete martensitic transformation and dissipating energy. It promotes the proliferation and redirection of shear bands at the interface between the Ta-rich phase and the B2-CuZr phase, delaying the generation of microcracks at the interface and introducing multiple shear bands, as shown in Fig. 6(c). Additionally, it generates a great amount of hard B19′-CuZr phase to compensate for the softening of the amorphous matrix, thereby enhancing the work-hardening effect of the composite.

In summary, the positive synergy effect between the Ta-rich phase and the B2-CuZr phase introduces a more complex stress field during deformation, which helps to dissipate energy and release stress concentrations through deformation in different stages and promotes the proliferation and redirection of shear bands. Additionally, it facilitates a more complete martensitic transformation in the B2-CuZr phase, resulting in a more pronounced work-hardening effect. The refined core-shell reinforcing structure obtained via dealloying in metallic melt should provide a great number of interfaces, which refers to those between the amorphous matrix and the B2-CuZr phase and

those between the core and shell phase. Such improvement in interface areas should further enhance the positive synergy effect from the hybrid reinforcing structure, making the samples show better mechanical performance compared with those produced via arc-melting process.

4 Conclusions

(1) The dealloying process refines the Ta-rich core effectively and thus decreases the size and homogenizes the distribution of the core-shell reinforcing phase.

(2) The refined core-shell hybrid structure reinforced BMGCs via dealloying process exhibits improved mechanical properties compared with that via arc-melting process. Ta5-De shows the highest plastic strain (11.6%) among all the samples. The advantage is pronounced compared with Ta5-Arc (4.3%).

(3) The refined core-shell hybrid-reinforcement structure provides a great area of interfaces, effectively hindering the rapid propagation of the main shear bands. Compared with the monolithic reinforcing structure, it exhibits unique synergy strengthening effects by introducing a more complex stress field during deformation.

CRediT authorship contribution statement

Wei GUO: Conceptualization, Funding acquisition, Investigation, Methodology, Resources, Writing – Review & editing; **Long-feng LI:** Data curation, Writing – Original draft; **Zhen ZHANG:** Data curation, Formal analysis; **Mi ZHAO:** Supervision, Writing – Review & editing; **Jin-cheng WANG:** Supervision; **Yan-qiang QIAO**, **Shu-lin LÜ** and **Shu-sen WU:** Investigation.

Declaration of competing interest

The authors declare that they have no known competing financial interests or personal relationships that could have appeared to influence the work reported in this paper.

Data Availability

The raw/processed data required to reproduce these findings cannot be shared at this time as the data also forms part of an ongoing study.

Acknowledgments

This work was supported by the National Natural Science Foundation of China (Nos. 52101138, 52201075), Natural Science Foundation of Hubei Province, China (Nos. 2023AFB798, 2022CFB614), Shenzhen Science and Technology Program, China (No. JCYJ20220530160813032), State Key Laboratory of Solidification Processing in NWPU, China (Nos. SKLSP202309, SKLSP202308), Guangdong Basic and Applied Basic Research Foundation, China (No. 2022A1515011227), and State Key Laboratory of Powder Metallurgy of Central South University, China (No. Sklpm-KF-05).

References

[1] INOUE A, ZHANG T, ISHIHARA S, SAIDA J, MATSUSHITA M. Preparation and mechanical properties of nanoquasicrystalline base bulk alloys [J]. Scripta Materialia, 2001, 44: 1615−1619.

[2] OKULOV I, SOLDATOV I, KABAN I, SARAC B, SPIECKERMANN F, ECKERT J. Fabrication of metastable crystalline nanocomposites by flash annealing of $Cu_{47.5}Zr_{47.5}Al_5$ metallic glass using joule heating [J]. Nanomaterials, 2020, 10: 84.

[3] ZHANG Ya-juan, KOU Sheng-zhong, LI Chun-yan, YUAN Xiao-peng, ZHAO Yan-chun, XU Jiao, PU Yong-liang. Effect of Zr content on glass-forming ability and mechanical properties of bulk metallic glasses [J]. Foundry, 2014, 63: 15−18.

[4] GUO Wei, YU Sheng, LÜ Shu-lin, WU Shu-sen, ZHAO Mi. Progress and prospect on amorphous alloy matrix composites [J]. Special Casting &. Nonferrous Alloys, 2022, 42: 661−671. (in Chinese)

[5] ZHAO Jin-bei, FAN Xin-hui, LI Bing, YANG Ke, KONG Yi-long, WANG Zhao. Microstructure and thermal expansion of copper-based amorphous alloys during structural relaxation [J]. China Foundry, 2020, 17: 8−14.

[6] SONG K K, PAULY S, WANG Z, KÜHN U, ECKERT J. Effect of TaW particles on the microstructure and mechanical properties of metastable $Cu4_{7.5}Zr_{47.5}Al_5$ alloys [J]. Materials Science and Engineering: A, 2013, 587: 372−380.

[7] WANG Xiao-peng, KONG Fan-tao. Resent development in high-entropy alloys and other high-entropy materials [J]. Journal of Aeronautical Materials, 2019, 39: 1−19.

[8] LIAO Y C, SONG S M, LI T H, CHIANG Y L, TSAI P H, NGUYEN V T, LI S Y, JANG J S C, HUANG J C. Significant TRIP-effect improvement by manipulating ZrCu-B2 distribution in ZrCuAlCo-based bulk metallic glass composites via inoculating Ta particles [J]. Journal of Alloys and Compounds, 2019, 774: 547−555.

[9] SHAO Yu-man, GUO Wei, LÜ Shu-lin, JIANG Wen-ming, WANG Jin-cheng, WU Shu-sen. Synthesis and mechanical behavior of in-situ porous Ti particle reinforced Mg−Cu−Gd−Ag bulk metallic glass matrix composite [J]. Journal of Alloys and Compounds, 2023, 967: 171842.

[10] GUO Wei, SAIDA J, ZHAO Mi, LÜ Shu-lin, WU Shu-sen. In-situ Ta-rich particle reinforced Zr-based bulk metallic glass matrix composites with tensile plasticity [J]. Journal of Alloys and Compounds, 2019, 775: 1002−1006.

[11] QIAO Ji-chao, LIU Xiao-di, WANG Qing, LIU C T, LU Jian, YANG Yong. Fast secondary relaxation and plasticity initiation in metallic glasses [J]. National Science Review, 2018, 5: 616−618.

[12] PAULY S, GORANTLA S, WANG G, KÜHN U, ECKERT J. Transformation-mediated ductility in CuZr-based bulk metallic glasses [J]. Nature Materials, 2010, 9: 473−477.

[13] WU Yuan, WANG Hui, WU Hong-hui, ZHANG Zhong-yan, HUI Xi-dong, CHEN Guo-liang, MA Dong, WANG Xun-li, LU Zhao-ping. Formation of Cu−Zr−Al bulk metallic glass composites with improved tensile properties [J]. Acta Materialia, 2011, 59: 2928−2936.

[14] ZHAI Hai-min, MA Xu, YUAN Hua-yan, OU Meng-jing, LI Wen-sheng. Research progress in control of microstructure and mechanical properties of in-situ bulk metallic glass composites [J]. Journal of Materials Engineering, 2022, 50: 78−89.

[15] CHENG Qi, HAN Xiao-liang, KABAN I, SOLDATOV I, WANG Wei-hua, SUN Yong-hao, ORAVA J. Phase transformations in a Cu−Zr−Al metallic glass [J]. Scripta Materialia, 2020, 183: 61−65.

[16] ZHANG Zhen, LÜ Shu-lin, WU Shu-sen, GUO Wei. Research progress on microstructural optimization of B2-CuZr phase reinforced amorphous alloy matrix composites [J]. Rare Metal Materials and Engineering, 2023, 52: 2253−2263. (in Chinese)

[17] GUO Wei, SHAO Yu-man, QIN Zhen-hua, LÜ Shu-lin, WU Shu-sen. Development of in-situ hybrid phase reinforced Mg-based metallic glass matrix composites [J]. Journal of Alloys and Compounds, 2020, 829: 154544.

[18] SHAO Yu-man, ZHENG Wei-jie, GUO Wei, LÜ Shu-lin, WU Shu-sen. In situ Fe-rich particle reinforced Mg-based metallic glass matrix composites via dealloying in metallic melt [J]. Materials Letters, 2021, 285: 129165.

[19] ZHAO Zhen-xiang, LI Chun-yan, LI Xin-ling, KOU Sheng-zhong. Effect of heat treatment and cryogenic thermal cycles on structure and properties of Zr-based bulk amorphous alloy [J]. The Chinese Journal of Nonferrous Metals, 2021, 31: 2185−2197. (in Chinese)

[20] GUO Wei, KATO H, YAMADA R, SAIDA J J. Fabrication and mechanical properties of bulk metallic glass matrix composites by in-situ dealloying method [J]. Journal of Alloys and Compounds, 2017, 707: 332−336.

[21] WU Fu-fa, CHAN K C, CHEN Shun-hua, JIANG Song-shan, WANG Gang. ZrCu-based bulk metallic glass composites with large strain-hardening capability [J]. Materials Science and Engineering A, 2015, 636: 502−506.

[22] FAN Cang, OTT R, HUFNAGEL T. Metallic glass matrix composite with precipitated ductile reinforcement [J]. Applied Physics Letters, 2002, 81: 1020−1022.

[23] ZHU Zheng-wang, ZHANG H, HU Zhuang-qi, ZHANG Wei, INOUE A. Ta-particulate reinforced Zr-based bulk metallic glass matrix composite with tensile plasticity [J]. Scripta Materialia, 2010, 62: 278−281.

[24] LIU Lin, CHAN K C, SUN Min, CHEN Qi. The effect of the addition of Ta on the structure, crystallization and mechanical properties of Zr−Cu−Ni−Al−Ta bulk metallic glasses [J]. Materials Science and Engineering: A, 2007, 445/446: 697−706.

[25] OKAZAKI K, ZHANG Wei, INOUE A. Microstructure and mechanical properties of $(Zr_{0.5}Cu_{0.4}Al_{0.1})_{100-x}Ta_x$ bulk metallic glass composites [J]. Materials Transactions, 2006, 47(10): 2571−2575.

[26] LIU Zeng-qian, LI Ran, LIU Gang, SU Wen-huang, WANG Hui, LI Yan, SHI Min-jie, LUO Xue-kun, WU Guo-juan, ZHANG Tao. Microstructural tailoring and improvement of mechanical properties in CuZr-based bulk metallic glass composites [J]. Acta Materialia, 2012, 60: 3128−3139.

[27] LIU Zeng-qian, WANG Hui, ZHANG Tao. Bulk metallic glass composites ductilized by core-shell structured dual crystalline phases through controlled inoculation [J]. Intermetallics, 2014, 45: 24−28.

[28] WADA T, SETYAWAN A D, YUBUTA K, KATO H. Nano- to submicro-porous β-Ti alloy prepared from dealloying in a metallic melt [J]. Scripta Materialia, 2011, 65: 532−535.

[29] HUANG Run-hua, ZHANG Zhen, GUO Wei, LÜ Shu-lin, WANG Jin-cheng, WU Shu-sen. Effects of Ta content on microstructure and properties of multi-phase reinforced CuZr based amorphous composites [J]. Special Casting &. Nonferrous Alloys, 2024, 44(2): 267−271. (in Chinese)

[30] ZHAI Hai-min, OU Meng-jing, YUAN Hua-yan, CUI Shuai, LI Wen-sheng. Research progress on work-hardening behavior of in-situ bulk metallic glass composites [J]. Materials Reports, 2022, 36: 138−146. (in Chinese)

[31] JIANG Song-shan, GAN K, HUANG Yong-jiang, XUE Peng, NING Zhing-liang, SUN Jian-fei, NGAN A H W. Stochastic deformation and shear transformation zones of the glassy matrix in CuZr-based metallic-glass composites [J]. International Journal of Plasticity, 2020, 125: 52−62.

[32] MA Guo-zhi, SUN Bao-an, PAULY S, SONG Kai-kai, KÜHN U, CHEN Ding, ECKERT J. Effect of Ti substitution on glass-forming ability and mechanical properties of a brittle Cu−Zr−Al bulk metallic glass [J]. Materials Science and Engineering: A, 2013, 563: 112−116.

[33] WU Yuan, MA Dong, LI Qi-kai, STOICA A, SONG Wen-li, WANG Hui, LIU Xing-jiang-jun, STOICA G, WANG Gong-yao, AN Ke, WANG Xun-li, LI M, LU Zhao-ping. Transformation-induced plasticity in bulk metallic glass composites evidenced by in-situ neutron diffraction [J]. Acta Materialia, 2017, 124: 478−488.

[34] SHAO Yu-man, ZHANG Zhen, GUO Wei, TANG Xue-feng, LÜ Shu-lin, CHEN Xiao-hua, WU Shu-sen. Development of Zr-based metallic glass matrix composites with hybrid reinforcing structures [J]. Intermetallics, 2021, 137: 107294.

[35] WANG Dong-mei, CHEN Yan, MU Juan, ZHU Zheng-wang, ZHANG Hai-feng, WANG Yan-dong, AN Ke. An in situ neutron diffraction study of plastic deformation in a $Cu4_{6.5}Zr_{46.5}Al_7$ bulk metallic glass composite [J]. Scripta Materialia, 2018, 153: 118−121.

[36] SHEN Yong, XU Jian. Improving plasticity and toughness of Cu−Zr−Y−Al bulk metallic glasses via compositional tuning towards the CuZr [J]. Journal of Materials Research, 2010, 25: 375−382.

[37] ZHU Yi-tian, LIU Yong, LI Fei, LIU Zu-ming, WU Hong. Preparation of $Zr_{50}Cu_{40}Al_{10}$ amorphous powder by mechanical alloying and its crystallization behaviors [J]. Materials Science and Engineering of Powder Metallurgy,

2010, 15: 64−69. (in Chinese)
[38] WANG Ming-zi, GUO Wei, LÜ Shu-lin, WU Shu-sen. Effect of deep cryogenic cycling treatment on structure and properties of metallic glass: A review [J]. Transactions of Nonferrous Metals Society of China. 2023, 33: 2879−2897.

基于金属熔体中脱合金反应细化核壳混杂增强 CuZr 基非晶复合材料

郭 威[1,2]，李龙丰[1]，张 震[1]，赵 觅[3,4]，王锦程[2]，乔彦强[2]，吕书林[1]，吴树森[1]

1. 华中科技大学 材料科学与工程学院 材料成形与模具技术全国重点实验室，武汉 430074；
2. 西北工业大学 凝固技术国家重点实验室，西安 710072；
3. 华中科技大学 航空航天学院，武汉 430074；
4. 深圳华中科技大学研究院，深圳 518057

摘 要：基于金属熔体中的脱合金反应成功制备成分为$[(Zr_{0.5}Cu_{0.5})_{0.925}Al_{0.07}Sn_{0.005}]_{100-x}Ta_x$ (原子分数，%，x=3, 5, 7)的非晶复合材料。该合金体系的增强相是以富 Ta 颗粒为核、B2-CuZr 为壳的核壳混合结构。该方法中，从 Zr−Ta 预合金中通过脱合金形成的 Ta 保持固态并聚集形成最终产物中的细小富 Ta 相。与传统电弧熔炼法通过熔解−沉淀形成的富 Ta 相相比，该方法可有效减小富 Ta 相尺寸。在 3 种成分中，$[(Zr_{0.5}Cu_{0.5})_{0.925}Al_{0.07}Sn_{0.005}]_{95}Ta_5$ 表现出最高塑性应变，达到 11.2%，远高于电弧熔炼对应样品的 4.3%。这种力学性能的改善源于细化的核壳混合增强结构，能更有效地阻碍主剪切带的快速扩展并促使其在界面处分枝增殖。

关键词：非晶复合材料；核壳混合增强结构；金属熔体中脱合金反应；强韧性；B2-CuZr

(Edited by Xiang-qun LI)